Nonlinear Optical Switching and Enhanced Nonlinear Optical Response of Au–CdSe Heteronanostructures

ARTICLE *in* THE JOURNAL OF PHYSICAL CHEMISTRY C · DECEMBER 2014

Impact Factor: 4.77 · DOI: 10.1021/jp5118739

4 AUTHORS, INCLUDING:

Sreeramulu Valligatla
Università degli Studi di Trento
15 PUBLICATIONS **62** CITATIONS
SEE PROFILE

Krishna Kanta Haldar
Central University of Punjab
16 PUBLICATIONS **399** CITATIONS
SEE PROFILE

Amitava Patra
Indian Association for the Cultivation of Science
172 PUBLICATIONS **4,148** CITATIONS
SEE PROFILE

THE JOURNAL OF PHYSICAL CHEMISTRY C

Article

pubs.acs.org/JPCC

Nonlinear Optical Switching and Enhanced Nonlinear Optical Response of Au−CdSe Heteronanostructures

V. Sreeramulu,[†] Krishna Kanta Haldar,[‡] Amitava Patra,*[,‡] and D. Narayana Rao*[,†]

[†]School of Physics, University of Hyderabad, Gachibowli, Hyderabad, 500046, India

[‡]Department of Materials Science, Indian Association for the Cultivation of Science, Jadavpur, Kolkata, 700032, India

Supporting Information

ABSTRACT: The metal−semiconductor heterostructures have recently emerged as a new class of functional materials for their potential applications due to plasmon-exciton interactions. Here, we demonstrate the nonlinear optical switching and enhanced nonlinear optical response of Au−CdSe heterostructures. The nonlinear optical properties of CdSe quantum dots and Au−CdSe heteronanostructures are investigated by using a *Z*-scan technique at 532 nm picosecond laser pulses, and 800 nm femtosecond laser pulses. Interestingly, we observe switching behavior from saturable absorption (SA) to reverse saturable absorption (RSA) with increasing laser intensity. The effective two-photon absorption cross section (σ_{eff}) of Au−CdSe heteronanostructures is greatly enhanced which is attributed to charge transfer between CdSe and Au nanoparticles. The nonlinear refraction changes its sign from positive to negative nonlinearity at higher intensities for Au−CdSe heterostructures. Third order nonlinear optical susceptibility is being measured by using the DFWM technique at 532 nm. Similar switching behavior is observed in Au−CdSe heteronanostructures at nonresonant excitations (800 nm), where a CdSe quantum dot shows reverse saturable absorption behavior attributed to the two-photon absorption. The optical switching behavior of these heterostructures could play a potential role in photonics and optoelectronic applications.

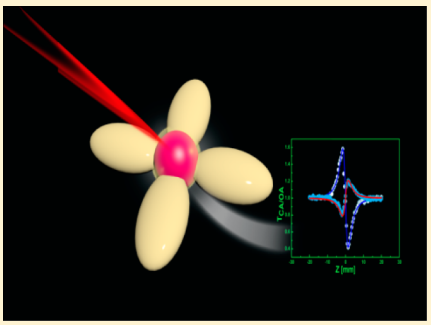

INTRODUCTION

Hybrid nanostructured materials based on metal nanoparticles and semiconductor quantum dots are emerging materials for future potential applications in various areas such as photonics and optoelectronics because of their functionalities.[1−7] Among the most prominent optical materials that are considered for future practical applications in photonics, metal−semiconductor hybrid nanostructures play a promising role because of their high optical nonlinearity and ultrafast time response.[8,9] The quantum confinement effects in semiconductors and dielectric confinement effects in metals make them a promising class of third order nonlinear materials, working at off-resonance as well as at resonance with fast response time.[10,11] Semiconductor quantum dots (QDs), with dimensions close to the Bohr radius of an electron−hole pair, have received tremendous attention owing to their unique physical and optical properties.[12]

Metal−semiconductor hybrid nanostructures, in which the metal component and the semiconductor counterpart are closely coupled in an effort to produce different functionalities, exhibit properties which are far beyond those of individual structures. Since parameters such as size, shape, and composition would highly affect the physical and optical properties of a hybrid system, the synthetic schemes of the metal−semiconductor hybrid have become more interesting.[7,13−15] Theoretical predictions have demonstrated the unique optical properties of metal−semiconductor hybrid structures toward various potential applications.[6,16] In the metal−semiconductor nanostructures, the nonlinear optical properties can be modified by the surface plasmon resonance (SPR) of the metal nanocrystals and the resultant local field environment.[17−19] Moreover, the plasmon-exciton interaction and the energy transfer among the hybrid system could result in modification of the nonlinear optical properties.[20] Recently, effective plasmon−exciton interaction-induced optical nonlinear enhancements in Au-CdS,[8] Ag-CdS,[21] core−shell structures, and Au-CdTe nanoparticle structures[9] are reported. Furthermore, Elim and his co-workers have demonstrated the intensity-dependent enhancement of saturable absorption in the PbS−Au hybrid nanocomposite.[22]

The charge transfer process between metal and semiconductor nanostructures could be expected to play an important role on the enhancement of nonlinear optical properties of metal−semiconductor heteronanostructures; however, the nonlinear optical properties of metal−semiconductor heteronanostructures with different sizes and shapes are rarely reported. The nonlinear optical properties of different materials depend on size and shape of their nanostructures. Moreover, the magnitude of enhancement is also strongly dependent on size, shape, and environment of the gold nanostructures. In particular, the synthesis of a metal−semiconductor materials with different size and shape is challenging, making it difficult to study their nonlinear optical

Received: November 29, 2014
Revised: December 2, 2014
Published: December 2, 2014

   dx.doi.org/10.1021/jp5118739 | *J. Phys. Chem. C* 2014, 118, 30333−30341

properties. In the present study, our motivation is to design Au−CdSe flower/tetrapod-shaped heteronanostructures with a Au core and CdSe arms and study their nonlinear optical properties. We have explored the nonlinear optical properties of CdSe and Au−CdSe using *Z*-scan and degenerate four wave mixing (DFWM) techniques at 532 nm wavelength in the picosecond regime and at 800 nm wavelength in the femtosecond regime.

EXPERIMENTAL PROCEDURES

Materials. Chloroauric acid ($HAuCl_4 \cdot 3H_2O$, 99.9%), cadmium oxide (CdO), selenium powder (Se), stearic acid (SA, 95%), oleic acid (OA, 96%), decanoic acid (DA, 98%), trioctylphosphine (TOP, 90%), trioctylphosphine oxide (TOPO, 99%), oleylamine (OAm, (98%), hexadecylamine (HDA, 90%), 1-octadecene (99%), tetraoctylammonium bromide (TOAB, Fluka), and 1-dodecylamine (DDA, 98%) were purchased from Aldrich, and sodium borohydride ($NaBH_4$), toluene (chemical grade), *n*-hexane (analytical grade), methanol (analytical grade), and ethanol (analytical grade) were purchased from Merck India, Ltd. All of the reagents were used without further purification. Seed Au particles were synthesized following the modified literature report[23,24] and these were purified, dissolved in toluene, and stored at room temperature. We have reported previously the detail synthesis of Au−CdSe heterostructures.[23,25] Using these Au particles as seeds, selenium and cadmium precursors were introduced to the reaction system at different reaction temperatures and time variations for the semiconductor CdSe nucleation and growth. To prevent separate CdSe nucleations, selenium precursors were injected prior to the cadmium precursors to the Au seed solution. In a typical reaction, the required amount of seed Au particles were dispersed in the noncoordinating solvent 1-octadecene along with the capping agent dodecylamine. The mixture was degassed, and then the reaction temperature was raised to the required temperature (200−280 °C) for CdSe growth. Flower-shaped heteronanostructures were formed when the cadmium stock solution was injected within a minute (<60 s) of Se introduction at 240 °C reaction temperature. However, tetrapod-shaped heteronanostructures were obtained with Au at the center when the reaction was carried out at 280 °C with the same reactant concentrations and the sequence of their injections. It is to be noted here that the initial gold seeds concentration remained the same for both the different nanostructures. CdSe QDs were synthesized in following the above reaction in the absence of Au nanoparticles.

The structural characteristics of the samples were obtained using a high resolution transmission electron microscope (HR-TEM) (JEOL-TEM-2010 operating voltage at 200 kV). The linear absorption spectra of the samples were measured using a UV−vis spectrophotometer (JASCO V-670). The samples were used as a solution which dissolved in chloroform, and the measurements were carried out in a quartz cuvette of 1 mm thickness. The third order nonlinear optical properties were investigated by using *Z*-scan technique with 532 nm picosecond laser pulses and 800 nm femtosecond laser pulses for CdSe quantum dot and Au−CdSe hybrid nanostructures. The picosecond laser is a frequency doubled, Q-switched Nd:YAG (Ekspla-2143A) laser, delivering 30 ps pulses at 532 nm with a repetition rate of 10 Hz. The femtosecond laser is a Spectra Physics Ti-sapphire regenerative amplifier delivering with 800 nm wavelength, operating at 1 kHz repetition rate and100 fs pulse width. The very popular *Z*-scan technique, which is a focused single beam method and translation of the sample across the focal point, was used for measuring both nonlinear refraction and nonlinear absorption.[26] A lens with focal length of 12 cm was used to focus the Gaussian beam, and the sample was moved through the beam waist of the laser beam over the length of 60 mm. At the focal point, the sample experiences maximum pump intensity, which gradually decreases in either direction from the focus. The sample solution taken in a 1 mm cuvette is smaller than the Rayleigh range of the focused beam, which is calculated to be ∼4 mm. The third order nonlinear optical susceptibility measurements were carried out using the degenerate four-wave mixing (DFWM) technique in a boxcar geometry (see Supporting Information).

RESULTS AND DISCUSSION

Figure 1 represents the high resolution transmission electron microscope (HR-TEM) images of the CdSe quantum dots and

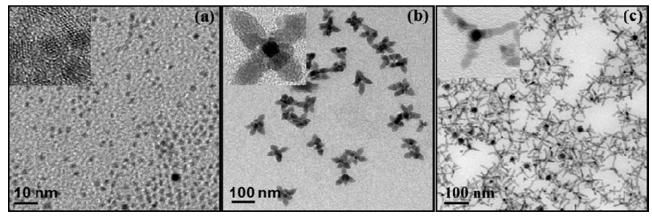

Figure 1. TEM images of (a) CdSe QDs nanocrystals, (b) Au−CdSe flower-shaped, and (c) tetrapod heteronanostructures. The inset pictures (in panels a, b, and c) show the corresponding high magnification images of CdSe QDs nanocrystals, Au−CdSe flower-shaped, and tetrapod heteronanostructures, respectively.

Au−CdSe heteronanostructures. It is clear from the TEM image (Figure 1a) that the CdSe nanoparticles are well disperse without aggregation. The particle size of CdSe was estimated to be ∼3 nm by using standard methods.[27,28] The inset shows the HRTEM image of CdSe QD nanocrystals (Figure 1a), and it is hexagonal in nature. Figure 1panels b and c show the TEM images of Au−CdSe flower-shaped and tetrapod heteronanostructures, respectively. From the TEM images it is clear that all the Au nanoparticles are well dispersed with almost a uniform size of ∼6 nm. The inset shows a single Au−CdSe flower shaped heteronanostructure (Figure 1b) with eight petal-type arms and the petals of these nanoflowers have an average arm length of approximately 30 nm. The magnified image clearly suggests that these arms are in different planes, that is, they are grown in different directions. The dark contrast of the Au core is visible in almost all cases. From the *d*-spacing it has been observed that CdSe petal arms are grown along the [0001] direction and with the progress of reaction they are also grown along the $\langle 2\bar{1}\bar{1}0 \rangle$ directions in addition to [0001]. The *d*-spacing of the planes at the center is 0.358 nm and it corresponds to the (0001) plane of wurtzite CdSe. Figure 1c shows the TEM image of tetrapod-shaped heteronanostructures. Maximum lengths of the arms of these tetrapods are up to 40 nm. The *d*-spacing of the planes at the center is 0.358 nm and it corresponds to the (0001) plane of wurtzite CdSe. A view of a tetrapod structure where the heterojunctions of the CdSe arm with gold seed is clearly seen in the inset.

Figure 2 shows the visible−near infrared (vis−NIR) absorption spectra of CdSe quantum dots and Au−CdSe heteronanostructures. We observed from the absorption measurements that the CdSe quantum dot shows the

dx.doi.org/10.1021/jp5118739 | J. Phys. Chem. C 2014, 118, 30333−30341

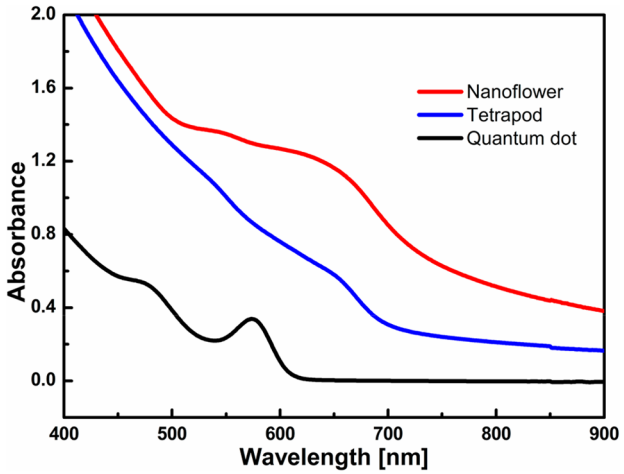

Figure 2. Linear absorption spectra of CdSe quantum dot and Au−CdSe flower-shaped heteronanostructure.

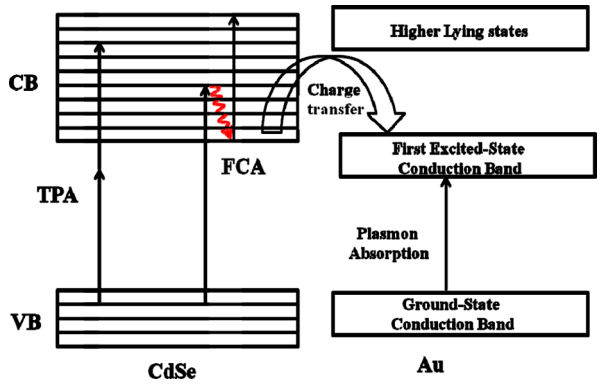

Figure 3. Schematic of energy level diagram for CdSe quantum dot and Au−CdSe heteronanostructures: (VB) valence band; (CB) conduction band; (TPA) two-photon absorption; (FCA) free carrier absorption.

absorption band at 576 nm. In the case of Au−CdSe heteronanostructures, it shows similar absorption spectra, but maximum absorption is broadened in the range of 500−700 nm, which is probably due to the overlap of the Au surface plasmon absorption with the absorption band of CdSe quantum dots in the metal−semiconductor heteronanostructures. The gold plasmonic absorption is around 540 nm[27] for 6 nm sized particles. In the present study, a spherical Au nanoparticle is in the center of the tetrapod, and flower heterostructures of Au−CdSe. Thus, the plasmonic mode of spherical nanoparticles is expected to be the same for all samples, but the change is due to Plasmon−exciton interaction.

Nonlinear Absorption Study at 532 nm Picosecond Laser. *Z*-scan measurements were carried out for all the samples in solution form filled in 1 mm quartz cuvette. The concentrations of the samples used in this measurement are 3.3×10^{-4} M and 2.3×10^{-6} M for CdSe quantum dot and Au−CdSe heteronanoflower and tetrapod, respectively. The linear transmittance of the samples at 532 nm are 72%, 34%, and 37% for CdSe, Au−CdSe flower shape, and tetrapod heteronanostructures, respectively. During the Z-scan measurement, it is observed that both the nonlinear absorption and nonlinear refraction are intensity-dependent. To investigate the intensity-dependent nonlinear absorption (NLA), we have performed the open aperture Z-scan experiment[26] at different input intensities. It is to be noted that we observe switching from saturable absorption (SA) to reverse saturable absorption (RSA) in both the samples with increasing laser intensity, and an increased nonlinear absorption is observed in the case of Au−CdSe heteronanostructures. We also carried out Z-scan measurements for the solvent at all the intensities used for the samples to remove the solvent contribution, and the results are shown in Figure S2 (Supporting Information). Here, we report the nonlinearities of CdSe and Au−CdSe by removing the solvent contribution from the samples.[29] Figure 3 represents the schematic energy level diagram for CdSe quantum dot and Au−CdSe heteronanostructures to explain the nonlinear processes.

Panels a, b, and c of Figure 4 represent the intensity-dependent nonlinear absorption curves for CdSe quantum dot, Au−CdSe flower shape, and tetrapod heteronanostructures, respectively, at different input intensities. Because of the resonant absorption at 532 nm, at relatively low input intensity of 8.75 GW/cm^2, all the samples possess strong SA behavior due to saturation in the ground state absorption as shown in Figure 4 panels a(i), b(i), and c(i) for CdSe and Au−CdSe heteronanostructures. Panels a(ii), b(ii), and c(ii) of Figure 4 represent the nonlinear absorption curves for CdSe and Au−CdSe heteronanostructures at the input intensity of 14 GW/cm^2. In the case of Au−CdSe heteronanostructures, the transmittance decreases when the sample moves closer to the focus point, a curve with two symmetrical humps with a valley appears, indicating SA followed by RSA behavior with increasing input intensity. Such type of switching behavior is observed in gold nanocubes,[30] Rhodmine6G-PVA solution,[31] Pt nanoparticles,[32] Cu_2O nanoparticles,[33] and also in Bi_2S_3@Au nanorods composites.[34]

Panels a(iii), b(iii), and c(iii) of Figure 4 represent the nonlinear absorptive curves for CdSe and Au−CdSe heteronanostructures, at the input intensity of 34 GW/cm^2. At higher input irradiance, they show SA behavior, when the sample is far away from the focal point (at low intensities) and the sample comes closer to the focal point (at high intensities), the resonant nonlinear absorption process dominates by taking the excited electron from the lower conduction band to the higher conduction band states through a second photon. This process is called free carrier absorption (FCA) or excited state absorption (ESA) leading to effective two-photon absorption (TPA) resulting in RSA behavior for both CdSe and Au−CdSe. At higher intensities, the saturation absorption of the lower excited states and FCA/ESA compete with each other. With further increase in the laser intensity, FCA/ESA dominates and reverse saturable absorption (RSA) occurs. In the present experiment, the critical amount of input intensities where the SA response is switched to RSA and the values are found to be 34 GW/cm^2 and 14 GW/cm^2, for CdSe and Au−CdSe flower-shape (tetrapod) heteronanostructures, respectively. The low input intensity to obtain SA over RSA in Au−CdSe is attributed to exciton−plasmon interactions in Au−CdSe.

The switchover from SA- to RSA-type of nonlinear behavior is explained by modeling the saturation of absorption of the lower band around 532 nm and direct two-photon absorption (TPA) from the ground state to excited state. The experimental data are therefore fitted by defining a nonlinear absorption coefficient $\alpha(I)$ which is a combination of saturable absorption and TPA terms,[30−33] through the relation

dx.doi.org/10.1021/jp5118739 | J. Phys. Chem. C 2014, 118, 30333−30341

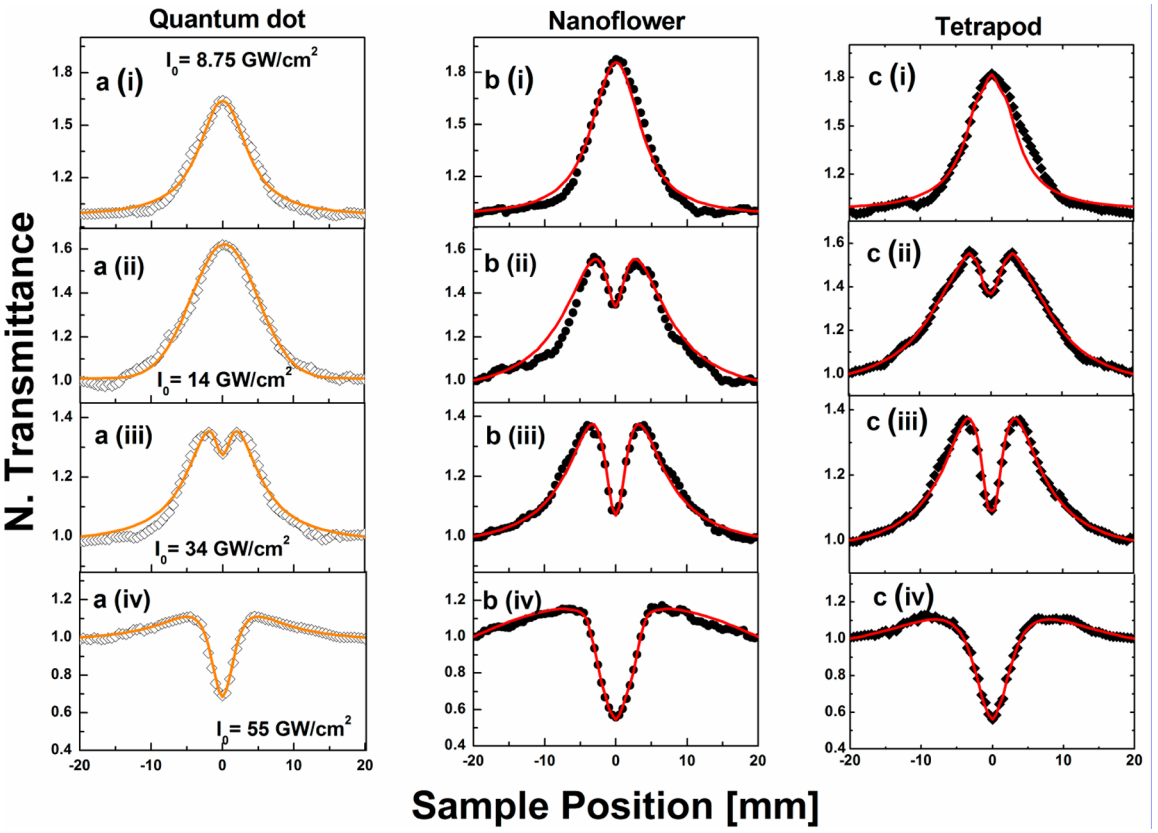

Figure 4. Intensity-dependent nonlinear absorption curves for (a) CdSe quantum dot, (b) Au−CdSe flower shape, and (c) Au−CdSe tetrapod heteronanostructures at different input intensities with 532 nm.

Table 1. Saturation Intensity (I_s), Nonlinear Absorption Coefficient (β_{eff}), Effective Two-Photon Absorption Cross Section (σ_{eff}) and Nonlinear Refractive Index (n_2) Values Obtained by Theoretical Fitting of Experimental Data for CdSe Quantum Dot and Au−CdSe Heteronanostructures at Different Input Intensities (I_0)[a]

	quantum dot				flower shape				tetrapod			
I_0	β_{eff}	I_s	σ_{eff}	n_2	β_{eff}	I_s	σ_{eff}	n_2	β_{eff}	I_s	σ_{eff}	n_2
55	0.22	56.7	0.041		0.49	76	13.2		0.46	79	12.1	
22		35		−0.32	0.15	12	4.1	−1.86	0.12	41	3.2	−1.75
1.72		1.2		−5.86		0.93		8.9		0.95		8.35
0.87		0.53		−6.53		0.43		12.8		0.48		12.4

[a] I_0, GW/cm^2; β_{eff}, cm/GW; I_s, GW/cm^2; n_2, (cm^2/W) × 10^{-14}; σ_{eff}, GM.

$$\alpha(I) = \frac{\alpha_0}{1 + I/I_s} + \beta_{eff} I \quad (1)$$

Here, the first term describes the SA, and second term describes TPA. α_0 is the linear absorption coefficient which is 3.4, 11.4, and 11.3 cm^{-1} at 532 nm for CdSe and Au−CdSe flower shape and tetrapod heteronanostructures, respectively. I is the laser intensity, β_{eff} is the effective TPA coefficient, which includes direct two-photon absorption and excited state absorption. Then, the normalized transmittance is given by,[32]

$$T(z) = \sum_{m=0}^{\infty} \frac{\left[\frac{\alpha I_0 L_{eff}}{1 + z^2/z_0^2}\right]^m}{m + 1} \quad (2)$$

Here, $L_{eff} = 1 - e^{-\alpha_0 L}/\alpha_0$, z is the longitudinal distance moved by the sample from the focus ($z = 0$), α is the nonlinear absorption coefficient, I_0 is the peak intensity at the focus, L_{eff} is the effective path length of the sample, and L is sample length, and z_0 is the Rayleigh range. The experimental data are fitted using a theoretical equation obtained by eq 1 and eq 2. The open aperture Z-scan traces are shown in Figure 4; the dotted lines represent the experimental data and the solid curves are the theoretical fittings obtained using eq 2.

As the input intensity further increases, the depth of the valley increases as shown in Figure 4 panels a(iv), b(iv), and c(iv) for CdSe quantum dot and Au−CdSe flower- and tetrapod-shaped heteronanostructures, respectively, at the input intensity of 55 GW/cm^2. The way the transition from SA to RSA occurs with an increase in the intensity for CdSe and Au−CdSe, it can be concluded that at higher intensities the nonlinear absorption term $I\beta_{eff}$ dominates in both CdSe and Au−CdSe leading to RSA behavior. The sharp nature of RSA at 55 GW/cm^2 for Au−CdSe indicates stronger TPA process.

The nonlinear optical parameters obtained from the experimental data by performing theoretical fits using eq 1 and 2 are listed in Table 1. It is seen that for 532 nm excitation, the values of β_{eff} and I_s are 0.22 cm/GW and 56.7 GW/cm^2 for CdSe quantum dot, and these values are changed to 0.49 cm/

dx.doi.org/10.1021/jp5118739 | J. Phys. Chem. C 2014, 118, 30333−30341

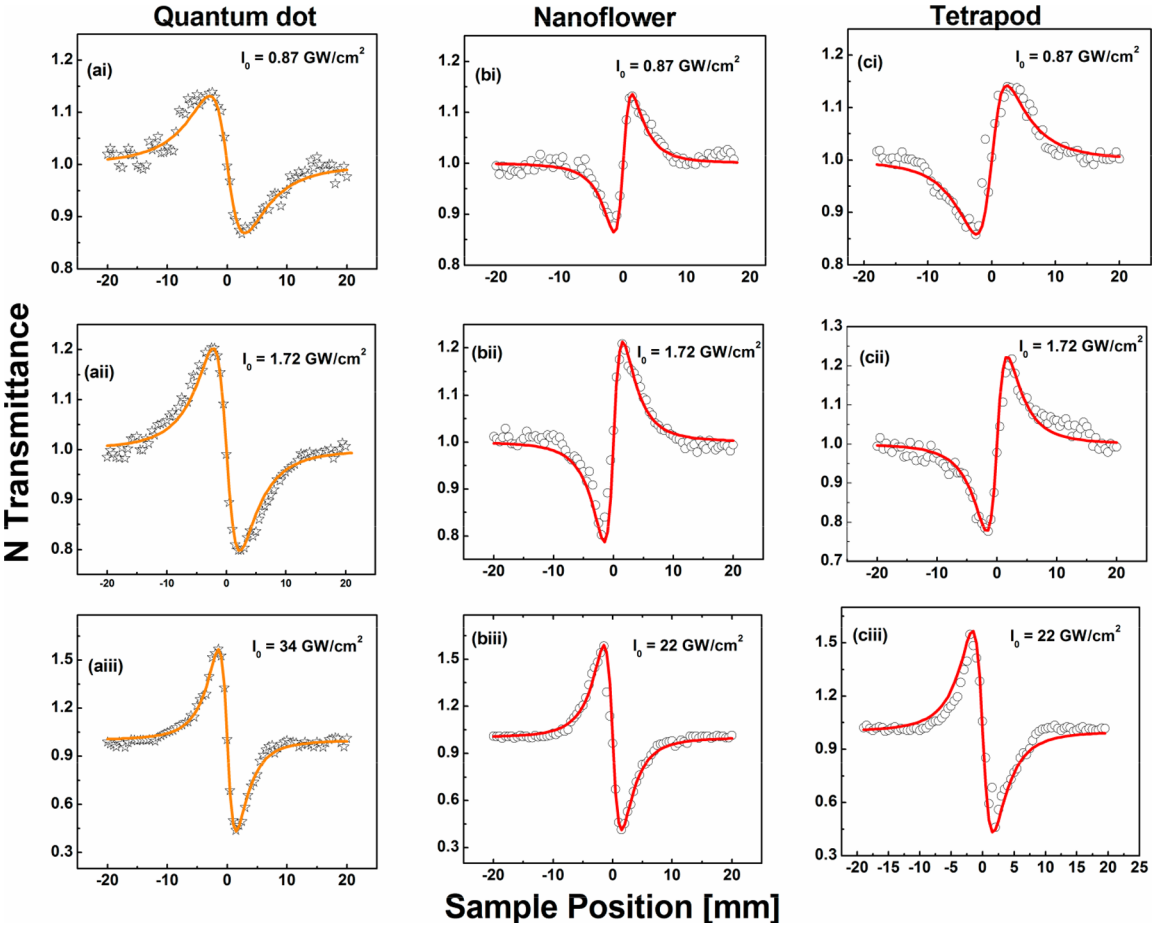

Figure 5. Closed aperture *Z*-scan traces for (a) CdSe quantum dot, (b) Au−CdSe flower shape, and (c) Au−CdSe tetrapod heteronanostructures at different input intensities with 532 nm.

GW and 76 GW/cm^2 and 0.46 cm/GW and 79 GW/cm^2 for Au−CdSe flower-shape and tetrapod heteronanostructures, respectively, at the input intensity of 55 GW/cm^2.

We have evaluated the effective two-photon absorption cross section (σ_{eff}) obtained using the relation $\sigma_{eff} = (h\upsilon/N)\,\beta_{eff}$. Where υ is the frequency of the laser pulse, N is the molar concentration, and β_{eff} is the effective two-photon absorption coefficient. The effective two-photon absorption cross section values are 0.041, 13, and 12 GM for CdSe quantum dot, Au−CdSe flower shape, and tetrapod heteronanostructures, respectively. It is observed that the effective two-photon cross section of the Au−CdSe flower shape and tetrapod heteronanostructures are 322 and 308 times higher than a single component of CdSe quantum dot. The photoluminescence quenching and shortening of lifetime of the Au−CdSe flower-shape and tetrapod heteronanostructures, and the enhancement in effective two-photon absorption cross section of Au−CdSe heteronanostructures is due to the charge transfer phenomena between CdSe quantum dot and the surface plasmons of Au nanoparticles.[4,25,26] It is reported that the enhancement of nonlinear absorption is observed for Bi_2S_3@Au nanorods composites, which is due to presence of surface plasmon resonance of Au nanoparticles.[34] Switching from SA to RSA of these samples is an interesting behavior which can be used for an optical pulse compressor, optical switching, and optical pulse narrowing,[35] and the enhancement of this switching behavior of Au−CdSe nanocomposites is expected to improve the optical device performance.

The nonlinear refraction studies are investigated through the closed and open aperture *Z*-scan technique with 532 nm picosecond laser pulses at different input intensities. The closed aperture Z-scan traces are shown in Figure 5 and the corresponding open aperture data are represented in Figure S3 (Supporting Information) for CdSe and Au−CdSe, respectively. Both samples show switchover from SA to RSA behavior at higher intensities and SA behavior at lower intensities, which is removed while calculating the nonlinear refraction as shown in Figure S2 (Supporting Information) by dividing the closed aperture data with open aperture data. Note that, we also carried out the *Z*-scan measurements on solvent (chloroform), and found that the solvent shows significant nonlinear absorption and refraction at higher intensities (Supporting Information) which is removed from the samples data.

To estimate the nonlinear refractive index of CdSe and Au−CdSe, first the normalized closed aperture transmittance (T_{CA}) was estimated using the relation given in ref 26. The nonlinear refractive index n_2 was calculated from the relation,[26]

$$n_2(\mathrm{cm^2W^{-1}}) = \frac{|\Delta\varphi|\lambda}{2\pi I_0 L_{eff}} \qquad (3)$$

where $\Delta\Phi$ is the phase change of the laser beam due to nonlinear refraction, λ is the wavelength of the laser beam, $L_{eff} = 1 - e^{-\alpha_0 L}/\alpha_0$ is the effective path length of the sample, L is the

dx.doi.org/10.1021/jp5118739 | J. Phys. Chem. C 2014, 118, 30333−30341

sample length, α_0 is the linear absorption coefficient, I_0 is the peak intensity.

The obtained nonlinear refractive index values for CdSe quantum dot and Au−CdSe heteronanostructures are given in Table 1. CdSe quantum dot exhibits a negative nonlinearity and the nonlinear refractive index value exhibits lower value at higher intensities even though CdSe shows stronger nonlinear absorption. The negative nonlinear refractive index can be concluded from the self-defocusing effect (the peak followed by valley) in CdSe quantum dots. The reduction of nonlinearity at higher intensities has no contribution from thermal nonlinearity. The nonlinearity is attributed predominantly to the electronic rather than to the thermal contribution because we carried out the experiment in the picoseconds time scale. At higher intensities, the effective two-photon absorption possibly leads to negative nonlinearity, and therefore decreases the total nonlinear refractive index. At lower intensities, SA behavior becomes predominant leading to larger nonlinear refractive index. In the case of Au−CdSe, it is very interesting to see a change of sign of nonlinear refraction from positive to negative nonlinearity as the intensity increases and also a decrease in the value of the refractive index. The positive contribution to the nonlinear refractive index is attributed to the electronic contribution of Au−CdSe flower/tetrapod-shaped heteronanostructures. The possible physical significance for the switchover from self-focusing to self-defocusing in Au−CdSe can be explained as follows. As discussed in the open aperture *Z*-scan results, at higher intensities, the charge transfer takes place from CdSe to Au nanoparticles in Au−CdSe heteronanostructures, which results in a large absorption cross section leading to thermal nonlinearity. At lower intensities, the free charge carriers are very low and pure electronic contribution dominates the nonlinear process leading to positive nonlinearity. There is a possibility that the electrons could transfer from d-band to s−p band in the Au nanoparticles, resulting in positive nonlinearity at low input intensities.

Ganeev et al. have observed a transformation of nonlinear refraction of Ag nanoparticles from self-defocusing to self-focusing which is unlike our system, and the nonlinear refractive index value decreases as the intensity increases.[36] Moreover, it is reported that the nonlinear refraction of Pd nanoparticles switches from self-defocusing to self-focusing which is attributed to interband transitions of electrons from d band to s−p conduction band in the Pd NPs.[37] To the best of our knowledge, this is the first report on switching behavior of nonlinear refraction in metal−semiconductor heteronanostructures. At lower intensities, a significant increase in the nonlinear refractive index of Au−CdSe compared to CdSe was observed. The increase in the nonlinearity from CdSe to Au−CdSe could be attributed to the plasmons in Au nanoparticles leading to intense local fields. The nonlinear switching behavior of Au−CdSe heterostructure is due to exciton−plasmon interactions. Such switching behavior plays an important role in optical signal processing.

Third Order Nonlinear Optical Susceptibility Using 532 nm Picosecond Laser. The third order nonlinear optical susceptibility, $\chi^{(3)}_{\text{sample}}$ measurements were carried out using DFWM technique with 532 nm, 30 ps laser pulses. The values of $\chi^{(3)}_{\text{sample}}$, for CdSe quantum dot and Au−CdSe flower-shape and tetrapod heteronanostructures have been measured by comparing the DFWM signal of the samples with that of chloroform as reference ($\chi^{(3)}_{\text{reference}} = 6.9 \times 10^{-14}$ esu[38,39]) for picosecond pulses which is in turn deduced from CS_2 ($\chi^{(3)}_{CS_2} = 6.3 \times 10^{-13}$ esu[38−40]). The following relationship is used to determine the sample $\chi^{(3)}_{\text{sample}}$,[40]

$$\chi^{(3)}_{\text{sample}} = \left(\frac{n_{\text{sample}}}{n_{\text{ref}}}\right)^2 \left(\frac{I_{\text{sample}}}{I_{\text{ref}}}\right)^{1/2} \left(\frac{L_{\text{sample}}}{L_{\text{ref}}}\right) \times \alpha L_{\text{sample}} \left(\frac{e^{\alpha L_{\text{sample}}/2}}{1 - e^{-\alpha L_{\text{sample}}}}\right) \chi^{(3)}_{\text{ref}} \quad (4)$$

where I is the DFWM signal intensity, α is the linear absorption coefficient, L is sample path length, and n is the refractive index. As the sample concentration is very low, the refractive index of chloroform (n = 1.446) is taken as the refractive index of the solution. The calculated third order nonlinear susceptibility ($\chi^{(3)}$) values are 1.37×10^{-13}, 5.45×10^{-13}, and 5.27×10^{-13} esu for CdSe, Au−CdSe flower-shape, and tetrapod heteronanostructures, respectively. The DFWM measurements were carried out at sufficiently low input intensities that the samples do not show any two-photon absorption. DFWM signals as a function of different input intensities for CdSe and Au−CdSe are shown in Figure 6. A slope of ∼3 obtained for all the samples indicates that the signals observed are from the third order nonlinear process. The origin for the DFWM signal is purely electronic contribution.

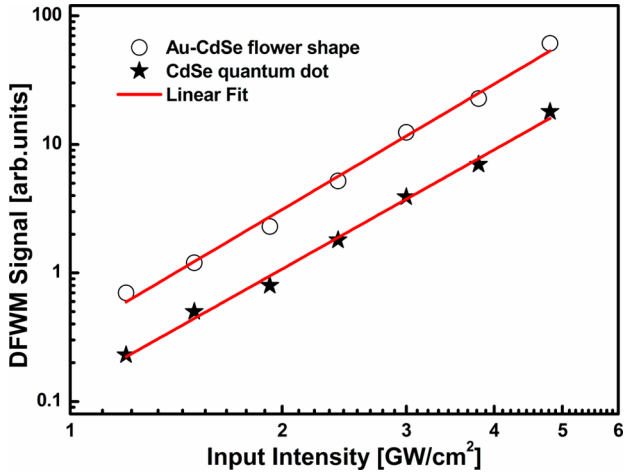

Figure 6. DFWM signal recorded for Au−CdSe flower-shaped heteronanostructure and CdSe quantum dot as a function of input intensity. The slopes for the Au−CdSe flower-shaped heteronanostructure and CdSe quantum dot are 3.22 and 3.07, respectively.

NLO Properties with 800 nm Femtosecond Laser. We have investigated the nonlinear optical properties of the CdSe quantum dot, Au−CdSe flower-shape, and tetrapod heteronanostructures in chloroform using an open aperture *Z*-scan technique with 100 fs pulse width, 800 nm wavelength which is far away from the surface plasmon resonance of Au nanoparticles. In this measurement, the excitation intensity at the focus varies from 66 GW/cm^2 to 225 GW/cm^2. The linear absorption coefficient at 800 nm for CdSe, Au−CdSe flower-shape and Au−CdSe tetrapod are 2.9, 8.4, and 8.6 cm^{-1} respectively. The solvent shows significant nonlinear absorption which is removed from the sample contribution (Supporting Information, Figure S6). Figure 7 represents the intensity-dependent nonlinear absorption properties of CdSe and Au−CdSe flower-shape and tetrapod heteronanostructures. The normalized open aperture *Z*-scan traces for CdSe quantum dots

dx.doi.org/10.1021/jp5118739 | J. Phys. Chem. C 2014, 118, 30333−30341

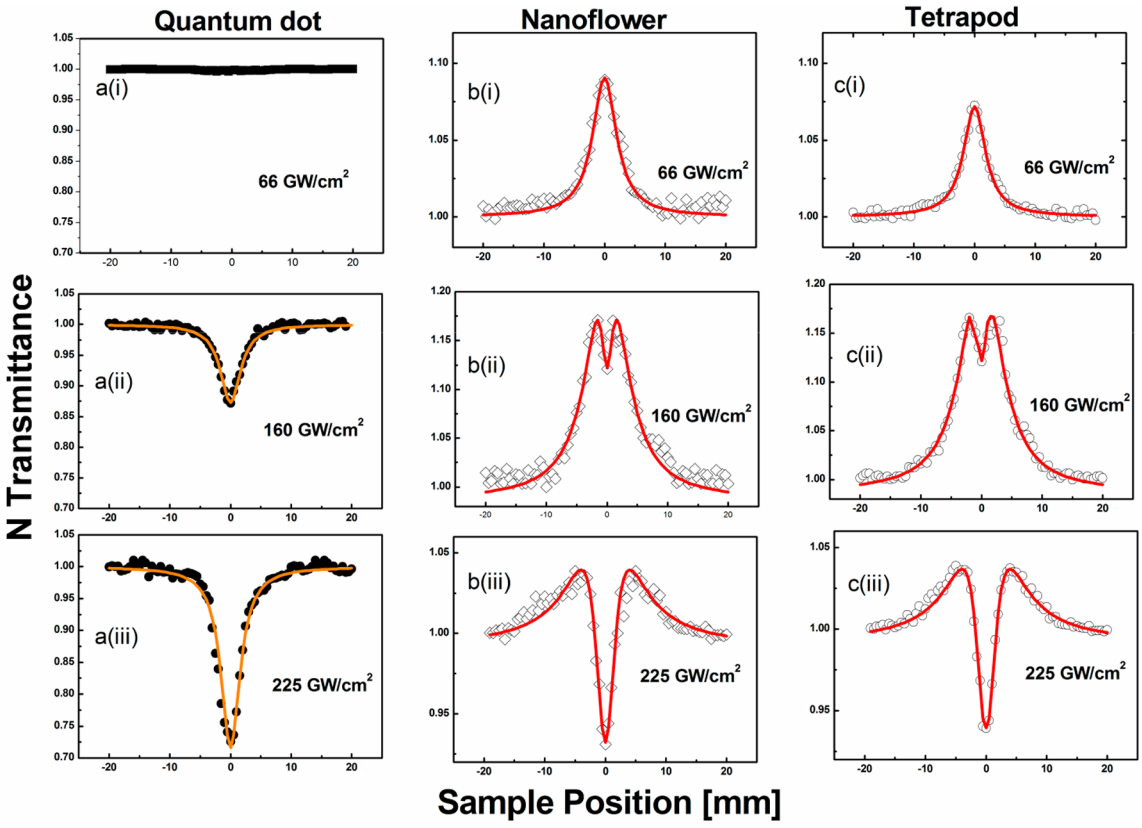

Figure 7. Intensity-dependent nonlinear absorption curves for (a) CdSe quantum dot, (b) Au−CdSe flower-shape, and (c) tetrapod heteronanostructures at different input intensities with 800 nm.

are shown in Figure 7a. At the input intensity of 66 GW/cm^2, there is no nonlinear absorption. At higher input intensity, it shows significant RSA behavior which is attributed to the two-photon absorption and this behavior increases as the input intensity increases as displayed in Figure 7a. Similar switching from SA to RSA behavior was observed for Au−CdSe heteronanostructures at 800 nm excitation. At lower intensities, Au−CdSe shows SA behavior which could possibly be due to the longer excited-state lifetimes. At the higher input intensities, when the sample is away from the focal point (lower intensities), the sample shows the SA behavior. When the sample moves closer to the focal point (higher intensities), the two-photon absorption dominates. As a result, a switch over from SA to RSA behavior is observed in Au−CdSe heteronanostructures at 160 GW/cm^2 is shown in Figure 7b(ii),c(ii). As the input intensity further increases, at 225 GW/cm^2 the two-photon absorption in CdSe quantum dot completely dominates the nonlinear process as shown in Figure 7b(iii),c(iii) for Au−CdSe heteronanostructures. The dotted lines are the experimental data, and the solid lines represent the theoretical fitting using the eqs 1 and 2. The two-photon absorption coefficient for CdSe quantum dot, Au−CdSe flower-shape and tetrapod heteronanostructures are 4.1 × 10^{-11}, 2.75 × 10^{-11}, and 2.54 × 10^{-11} esu, respectively, at the input intensity of 225 GW/cm^2.

The switching behavior is observed in Bi_2S_3@Au nanorod composites at the excitation of 532 nm and 1064 nm.[34] In our present system, it is interesting to observe a switching behavior in the Au−CdSe system, unlike the CdSe system at the excitation of 800 nm, which can find potential applications in optoelectronics. The nonlinear optical properties of flower-shape and tetrapod heteronanostructures are similar in both the picosecond and femtosecond areas. However, they show small differences in the parameters of nonlinear optical coefficients. Both composite structures contain Au as core and CdSe as the petal arm. The Au−CdSe flower-shape heteronanostructure has the eight arms of CdSe as compared to the tetrapod. Moreover, the possibility of efficient charge transfer from CdSe arms to Au core increases the NLO properties of the Au−CdSe flower-shape heteronanostructures.

CONCLUSION

In summary, we have reported the nonlinear optical properties of hybrid metal−semiconductor nanostructures using the *Z*-scan technique with 532 nm, picosecond laser pulses and 800 nm, femtosecond laser pulses. At resonant excitation, all the samples show switch over from SA to RSA behavior at 532 nm excitation. The effective two-photon absorption cross section of CdSe quantum dot, Au−CdSe flower-shape and tetrapod heteronanostructures are 0.041, 13.2, and 12.1 GM, respectively. The large enhancement in the effective two-photon absorption cross section is attributed to the charge transfer process between CdSe and Au nanoparticles. We observed a sign reversal in the nonlinear refraction and also an increase in its magnitude while going from CdSe to Au−CdSe. At 800 nm excitation, Au−CdSe heteronanostructures show the switching behavior unlike CdSe quantum dots. The results suggest that the Au−CdSe metal−semiconductor nanoheteronanostructures could play a potential role in photonics and optoelectronic applications.

dx.doi.org/10.1021/jp5118739 | J. Phys. Chem. C 2014, 118, 30333−30341

■ ASSOCIATED CONTENT

Supporting Information

The description of the degenerate four-wave mixing (DFWM) technique is given. Figure S2 shows the open aperture nonlinear absorption curves for chloroform (solvent) at different input intensities. Figure S3 shows the *Z*-scan open aperture traces for CdSe quantum dot and Au−CdSe flower-shaped heteronanostructures at different intensities. Figure S4 shows the closed aperture *Z*-scan traces for chloroform (solvent) at different input intensities at 532 nm excitation. Figure S5 represents the intensity dependence of DFWM signal at 532 nm for Au−CdSe tetrapod heteronanostructures. Figure S6 shows the *Z*-scan open aperture traces for the solvent at different intensities with 800 nm excitation. This material is available free of charge via the Internet at http://pubs.acs.org.

■ AUTHOR INFORMATION

Corresponding Authors

*E-mail: dnr.laserlab@gmail.com.

*E-mail: msap@iacs.res.in

Notes

The authors declare no competing financial interest.

■ ACKNOWLEDGMENTS

D.N.R. acknowledges the Department of Science and Technology, India, sponsored India-Trento and Indo-Australia collaboration projects for the financial support. A.P. is grateful for the DAE-SRC Award.

■ REFERENCES

(1) Vaneski, A.; Susha, A. S.; Rodríguez-Fernández, J.; Berr, M.; Jäckel, F.; Feldmann, J.; Rogach, A. L. Hybrid colloidal heterostructures of anisotropic semiconductor nanocrystals decorated with noble metals: Synthesis and function. *Adv. Funct. Mater.* **2011**, *21*, 1547−1556.

(2) Elmalem, E.; Saunders, A. E.; Costi, R.; Salant, A.; Banin, U. Growth of photocatalytic CdSe−Pt nanorods and nanonets. *Adv. Mater.* **2008**, *20*, 4312−4317.

(3) Li, Y. Q.; Guan, L. Y.; Zhang, H. L.; Chen, J.; Lin, S.; Ma, Z. Y.; Zhao, Y. D. Distance-dependent metal-enhanced quantum dots fluorescence analysis in solution by capillary electrophoresis and its application to DNA detection. *Anal. Chem.* **2011**, *83*, 4103−9.

(4) Kanta Haldar, K.; Kundu, S.; Patra, A. Non-radiative relaxation and rectification behavior of metal/semiconductor tetrapod heterostructures. *Appl. Phys. Lett.* **2014**, *104*, 063110.

(5) Costi, R.; Saunders, A. E.; Elmalem, E.; Salant, A.; Banin, U. Visible light-induced charge retention and photocatalysis with hybrid CdSe−Au nanodumbbells. *Nano Lett.* **2008**, *8*, 637−641.

(6) Achermann, M. Exciton−plasmon interactions in metal−semiconductor nanostructures. *J. Phys. Chem. Lett.* **2010**, *1*, 2837−2843.

(7) Soni, U.; Tripathy, P.; Sapra, S. Photocatalysis from fluorescence-quenched CdSe/Au nanoheterostructures: A size-dependent study. *J. Phys. Chem. Lett.* **2014**, *5*, 1909−1916.

(8) Nan, F.; Liang, S.; Liu, X.-L.; Peng, X.-N.; Li, M.; Yang, Z.-J.; Zhou, L.; Hao, Z.-H.; Wang, Q.-Q. Sign-reversed and magnitude-enhanced nonlinear absorption of Au−CdS core−shell heteronanorods. *Appl. Phys. Lett.* **2013**, *102*, 163112.

(9) Fu, M.; Wang, K.; Long, H.; Yang, G.; Lu, P.; Hetsch, F.; Susha, A. S.; Rogach, A. L. Resonantly enhanced optical nonlinearity in hybrid semiconductor quantum dot−metal nanoparticle structures. *Appl. Phys. Lett.* **2012**, *100*, 063117.

(10) Gao, Y.; Huong, N. Q.; Birman, J. L.; Potasek, M. J. Large nonlinear optical properties of semiconductor quantum dot arrays embedded in an organic medium. *J. Appl. Phys.* **2004**, *96*, 4839.

(11) Kim, S.; Jin, J.; Kim, Y. J.; Park, I. Y.; Kim, Y.; Kim, S. W. High-harmonic generation by resonant plasmon field enhancement. *Nature* **2008**, *453*, 757−60.

(12) Reiss, P.; Protiere, M.; Li, L. Core/shell semiconductor nanocrystals. *Small* **2009**, *5*, 154−68.

(13) Zhang, J.; Tang, Y.; Lee, K.; Ouyang, M. Nonepitaxial growth of hybrid core-shell nanostructures with large lattice mismatches. *Science* **2010**, *327*, 1634−8.

(14) Li, M.; Yu, X.-F.; Liang, S.; Peng, X.-N.; Yang, Z.-J.; Wang, Y.-L.; Wang, Q.-Q. Synthesis of Au-CdS core−shell hetero-nanorods with efficient exciton-plasmon interactions. *Adv. Funct. Mater.* **2011**, *21*, 1788−1794.

(15) Li, Z.; Hu, Y.; Sun, Y. Promoting photocatalytic multiple-electron reduction in aerobic solutions using Au-tipped CdSe nanorod clusters. *Chem. Commun.* **2014**, *50*, 1411−3.

(16) Liu, X. N.; Yao, D. Z.; Zhou, H. M.; Chen, F.; Xiong, G. G. Third-order nonlinear optical response in quantum dot−metal nanoparticle hybrid structures. *Appl. Phys. B: Laser Opt.* **2013**, *113*, 603−610.

(17) Pu, Y.; Grange, R.; Hsieh, C.-L.; Psaltis, D. Nonlinear optical properties of core−shell nanocavities for enhanced second-harmonic generation. *Phys. Rev. Lett.* **2010**, *104*, 207402.

(18) Yang, Y.; Nogami, M.; Shi, J.; Chen, H.; Liu, Y.; Qian, S. Ultrafast electron dynamics and enhanced optical nonlinearities of CdS-capped Au/$BaTiO_3$ composite film. *J. Appl. Phys.* **2005**, *98*, 033528.

(19) Singh, M. R. Enhancement of the second-harmonic generation in a quantum dot−metallic nanoparticle hybrid system. *Nanotechnology* **2013**, *24*, 125701.

(20) Ma, G. H.; He, J.; Rajiv, K.; Tang, S. H.; Yang, Y.; Nogami, M. Observation of resonant energy transfer in Au:CdS nanocomposite. *Appl. Phys. Lett.* **2004**, *84*, 4684.

(21) Gong, H. M.; Wang, X. H.; Du, Y. M.; Wang, Q. Q. Optical nonlinear absorption and refraction of CdS and CdS−Ag core−shell quantum dots. *J. Chem. Phys.* **2006**, *125*, 24707.

(22) Elim, H. I.; Ji, W.; Yang, J.; Lee, J. Y. Intensity-dependent enhancement of saturable absorption in PbS−Au_4 nanohybrid composites: Evidence for resonant energy transfer by Auger recombination. *Appl. Phys. Lett.* **2008**, *92*, 251106.

(23) Haldar, K. K.; Pradhan, N.; Patra, A. Formation of heteroepitaxy in different shapes of Au−CdSe metal-semiconductor hybrid nanostructures. *Small* **2013**, *9*, 3424−32.

(24) Prasad, B. L. V.; Stoeva, S. I.; Sorensen, C. M.; Klabunde, K. J. Digestive-ripening agents for gold nanoparticles: Alternatives to thiols. *Chem. Mater.* **2003**, *15*, 935−942.

(25) Haldar, K. K.; Sinha, G.; Lahtinen, J.; Patra, A. Hybrid colloidal Au−CdSe pentapod heterostructures synthesis and their photocatalytic properties. *ACS Appl. Mater. Interfaces* **2012**, *4*, 6266−6272.

(26) Sheik-Bahae, M.; Said, A. A.; Wei, T. H.; Hagan, D. J.; Van Stryland, E. W. Sensitive measurement of optical nonlinearities using a single beam. *IEEE J. Quantum Electron.* **1990**, *26*, 760−769.

(27) Haldar, K. K.; Sen, T.; Patra, A. Metal conjugated semiconductor hybrid nanoparticle-based fluorescence resonance energy transfer. *J. Phys. Chem. C* **2010**, *114*, 4869−4874.

(28) Moffitt, M.; Eisenberg, A. Size control of nanoparticles in semiconductor-polymer composites. 1. Control via multiplet aggregation numbers in styrene-based random ionomers. *Chem. Mater.* **1995**, *7*, 1178−1184.

(29) Bala Murali Krishna, M.; Narayana Rao, D. Influence of solvent contribution on nonlinearities of near infra-red absorbing croconate and squaraine dyes with ultrafast laser excitation. *J. Appl. Phys.* **2013**, *114*, 133103.

(30) Lee, Y. H.; Yan, Y.; Polavarapu, L.; Xu, Q.-H. Nonlinear optical switching behavior of Au nanocubes and nano-octahedra investigated by femtosecond *Z*-scan measurements. *Appl. Phys. Lett.* **2009**, *95*, 023105.

(31) Nithyaja, B.; Misha, H.; Radhakrishnan, P.; Nampoori, V. P. N. Effect of deoxyribonucleic acid on nonlinear optical properties of

Rhodamine 6G-polyvinyl alcohol solution. *J. Appl. Phys.* **2011**, *109*, 023110.
(32) Gao, Y.; Zhang, X.; Li, Y.; Liu, H.; Wang, Y.; Chang, Q.; Jiao, W.; Song, Y. Saturable absorption and reverse saturable absorption in platinum nanoparticles. *Opt. Commun.* **2005**, *251*, 429−433.
(33) Sekhar, H.; Narayana Rao, D. Preparation, characterization and nonlinear absorption studies of cuprous oxide nanoclusters, micro-cubes and micro-particles. *J. Nanopart. Res.* **2012**, *14*, 1−11.
(34) Chen, J. L. T.; Nalla, V.; Kannaiyan, G.; Mamidala, V.; Ji, W.; Vittal, J. J. Synthesis and nonlinear optical switching of Bi_2S_3 nanorods and enhancement in the NLO response of Bi_2S_3@Au nanorod-composites. *New J. Chem.* **2014**, *38*, 985−992.
(35) Band, Y. B.; Harter, D. J.; Bavli, R. Optical pulse compressor composed of saturable and reverse saturable absorbers. *Chem. Phys. Lett.* **1986**, *126*, 280−284.
(36) Ganeev, R. A.; Ryasnyansky, A. I.; Stepanov, A. L.; Usmanov, T. Saturated absorption and nonlinear refraction of silicate glasses doped with silver nanoparticles at 532 nm. *Opt. Quantum Electron.* **2004**, *36*, 949−960.
(37) Fan, G.; Qu, S.; Wang, Q.; Zhao, C.; Zhang, L.; Li, Z. Pd nanoparticles formation by femtosecond laser irradiation and the nonlinear optical properties at 532 nm using nanosecond laser pulses. *J. Appl. Phys.* **2011**, *109*, 023102.
(38) Srivastava, P. C.; Singh, V.; Dwivedi, S.; Pujan, T.; Bhuj, A. K.; Butcher, R. J.; Bala Murali Krishna, M.; Narayana Rao, D. Synthesis, crystal structure, supramolecular associations and third-order non-linear optical (NLO) properties of some organotellurium (IV) derivatives. *Polyhedron* **2012**, *42*, 36−42.
(39) Srivastava, P. C.; Dwivedi, S.; Singh, V.; Pujan, T.; Bhuj, A. K.; Butcher, R. J.; Krishna, M. B. M.; Rao, D. N. Supramolecular assemblies of organotellurium(IV) dithiocarbamates and third order nonlinear optical susceptibility ($\chi^{(3)}$) of $C_4H_7(CH_3)Te[S_2CN(C_2H_5)_2]_2$. *Inorg. Chim. Acta* **2012**, *388*, 175−183.
(40) Wu, J.; Yan, J.; Sun, D.; Li, F.; Zhou, L.; Sun, M. Third-order nonlinear optical property of a polyphenylene oligomer: poly(2,5-dialkozyphenylene). *Opt. Commun.* **1997**, *136*, 35−38.